Available online at www.sciencedirect.com

ScienceDirect

Geochimica et Cosmochimica Acta 140 (2014) 199–211

Geochimica et Cosmochimica Acta

www.elsevier.com/locate/gca

Kinetics of ikaite precipitation and dissolution in seawater-derived brines at sub-zero temperatures to 265 K

Stathys Papadimitriou [a,*], Hilary Kennedy [a], Paul Kennedy [a], David N. Thomas [a,b]

[a] Ocean Sciences, College of Natural Sciences, Bangor University, Menai Bridge, Anglesey LL59 5AB, UK
[b] Finnish Environment Institute (SYKE), Marine Research Centre, FI-00251 Helsinki, Finland

Received 30 October 2013; accepted in revised form 18 May 2014; available online 2 June 2014

Abstract

The kinetics of calcium carbonate hexahydrate (ikaite) precipitation and dissolution were investigated in seawater and seawater-derived brines at sub-zero temperatures using the constant addition experimental technique. The steady state rate of these two processes was found to be a function of the deviation of the solution from equilibrium with respect to ikaite and conformed to the same empirical rate law as the anhydrous $CaCO_3$ polymorphs, calcite and aragonite. In addition to the saturation state of the brine with respect to ikaite, the salinity of the brine and the temperature of the reaction evidently exerted some control on the ikaite precipitation kinetics, while the dissolution kinetics of the polymorph were not noticeably influenced by these two parameters. The experimental salinity and temperature conditions were equivalent to those at thermal equilibrium between brine and ice in the sea ice cover of polar seas. Simple modelling of the CO_2 system by extrapolation of the oceanic equivalent to sea ice brines showed that the physical concentration of seawater ions and the changes in ikaite solubility as a function of salinity and temperature, both inherent in the sea ice system, would be insufficient to drive the emergent brines to ikaite supersaturation and precipitation in sea ice down to −8 °C. The loss of dissolved inorganic carbon to the gas phase of sea ice and to sympagic autotrophs are two independent mechanisms which, in nature, could prompt the brine CO_2 system towards ikaite supersaturation and precipitation. Under these conditions, the steady state precipitation rate of ikaite was found to be fast enough for rapid formation within short time scales (days to weeks) in sea ice. The observed ikaite dissolution kinetics were also found conducive to short turn-over time scales of a few hours to a few days in corrosive solutions, such as surface seawater.

1. INTRODUCTION

Recent field collections have documented the presence of ikaite ($CaCO_3 \cdot 6H_2O$) in sea ice of the high latitude oceans (Dieckmann et al., 2008; Dieckmann et al., 2010; Rysgaard et al., 2012; Fischer et al., 2013; Rysgaard et al., 2013). The occurrence of this hydrated $CaCO_3$ polymorph in sea ice has added an, as yet, poorly-understood abiotic component to the well-documented biological cycling of carbon by sympagic organisms (Arrigo et al., 1997; Arrigo et al., 2010; Deming, 2010).

During sea ice formation and growth, the dissolved salts in the parent seawater are excluded from the ice crystal matrix and become concentrated in the residual liquid (brine), part of which is trapped in pockets and channels in the ice matrix (Cox and Weeks, 1983; Petrich and Eicken, 2010). As a result, brine salinity increases as a function of decreasing ice temperature from the freezing point of seawater (−1.85 °C at a salinity of 35 and 1 atm total pressure) near the ice–seawater interface to colder

* Corresponding author. Tel.: +44 1248 383641; fax: +44 1248 716367.
E-mail address: s.papadimitriou@bangor.ac.uk (S. Papadimitriou).

http://dx.doi.org/10.1016/j.gca.2014.05.031
0016-7037/

temperatures in the upper parts of the ice column in the transition from summer to winter, and vice versa in the transition from winter to summer. The variation in the ionic strength and temperature of the brine inclusions during the formation–decay cycle of sea ice perturbs the thermodynamic solid–solution equilibrium of carbonate, sulphate, and chloride salts, initiating their sequential precipitation and dissolution cycles in the brine as a function of ice temperature (Marion, 2001). Ikaite is included in this sequence of authigenic solid phases in sea ice under conditions of sufficiently low concentration of dissolved carbon dioxide [here, expressed in partial pressure format (pCO_2)] (Marion, 2001; Papadimitriou et al., 2013). Shifts in brine pCO_2 are inherent in the sea ice formation–decay process, also as a result of the perturbation of the thermodynamic equilibria amongst the dissolved CO_2 species [collectively, total dissolved inorganic carbon (C_T)] in the brine. Such shifts are inversely related to temperature and will result in a progressive brine pCO_2 rise above the current atmospheric value as ice temperature drops during sea ice formation and growth (Miller et al., 2011a,b; Geilfus et al., 2012). The resulting disequilibrium relative to atmospheric pCO_2 will promote transfer of dissolved CO_2 to the gas phase of sea ice with concomitant lowering of the brine pCO_2 (brine CO_2 degassing) (Papadimitriou et al., 2004). Uptake of C_T by the sympagic autotrophs also causes dramatic reductions in brine pCO_2 to values below atmospheric equilibrium (Gleitz et al., 1995; Papadimitriou et al., 2007; Delille et al., 2007).

Sea ice and, with it, the potential areal extent of ikaite occurrence in the oceanic environment stretch over several million square kilometers in the polar oceans and sup-polar seas. As a first step towards the quantification of ikaite dynamics in sea ice, its concentration-based equilibrium solubility constant has been determined in salinity–temperature pairs matching the ice–brine thermal equilibrium down to -7.5 °C (Papadimitriou et al., 2013). The kinetics of the precipitation–dissolution cycle of this polymorph now need to be studied in similar salinity and temperature conditions before a true appreciation of its role in the polar oceanic carbon cycling can be determined. The direct field evidence for ikaite authigenesis in sea ice can hardly address the scale of ikaite production in the sea ice cover and the fate of the polymorph during sea ice decay without kinetic information. Such information will allow full integration of the ikaite cycle into existing geochemical models of sea ice, such as the FREZCHEM (Marion, 2001) and the coupled physical-biological model in Arrigo et al. (1997). Therefore, the aim of this study was to provide the first kinetic data of ikaite precipitation and dissolution at the sub-zero temperatures and high salinities typical of sea ice brines via seeded experiments at constant pCO_2 (open system).

2. MATERIALS AND METHODS

2.1. The constant addition technique

The reaction kinetics of the precipitation and dissolution of ikaite were investigated in seeded open system experiments with the constant addition technique (Zhong and Mucci, 1993; Zuddas et al., 2003). The technique allows the investigation of solid–solution reaction kinetics in a steady state environment as demonstrated in Zhong and Mucci (1993). It involves the addition of a constant composition solution (reacting solution) at a constant delivery rate into a 500 mL glass reaction vessel (reactor), loaded with mineral particles (seed). The reacting solution (in this study, seawater and seawater-derived brine) was delivered in a Tygon tubing (0.64 mm ID) to the top of the reactor using a peristaltic pump (Watson Marlow 520U). The delivery rate of the reacting solution was determined gravimetrically after every experiment using distilled water. The total amount of reacting solution delivered per experiment throughout this study was 114 ± 6 g ($n = 31$). Synthetic ikaite was used to seed the reaction and was prepared with the method of Bischoff et al. (1993) as reported in detail in Papadimitriou et al. (2013). Approximately 0.3 g of synthetic ikaite was introduced into the cold reactor, with an overall average of 0.303 ± 0.002 g ($n = 31$), equivalent to 2915 ± 21 μmol carbonate alkalinity and a solid to solution ratio of 2.7 g kg^{-1} at the end of each experiment. The solution-seed mixture was continuously purged with a water-saturated CO_2/N_2 gas mixture with a certified CO_2 composition (in ppm, equivalent to μmol/mol; uncertainty ⩽5%, BOC, boc.com) through a frit at the bottom of the reactor, provided at a controlled rate (200–400 mL/min) via a CHELL CMD100 microprocessor controller and Hastings Mass Flow Control Valve. The certified CO_2 composition of the CO_2/N_2 mixture was converted to partial pressure (pCO_2, in μatm) using 1 atm total pressure. The reaction thus proceeded at a constant pCO_2. Altering the reaction pCO_2 per experiment provided a means of monitoring the extent of saturation of the reacting solution with respect to ikaite.

Seawater was used both as the reacting solution and for the preparation of the experimental brines by its variable freezing. The brines were filtered through pre-combusted (500 °C, 3 h) GF/F filters (0.7 μm, WHATMAN) and were kept stored in acid-washed glass bottles at room temperature (stock reacting solutions). The pCO_2 of the prepared brines was likely to be much higher (see Section 4.3) than the atmospheric value of approximately 390 μatm due to the physical concentration of solutes present in the parent seawater during freezing. For this reason, the reacting solutions were pre-equilibrated for 10–72 h with a pCO_2 close to that maintained in the reactor during the experiments but never below 390 μatm, to avoid $CaCO_3$ precipitation in the Tygon tubing during delivery in the reactor.

During each experiment, the reacting solution, the gas hydrator, and the reactor were immersed in a constant-temperature water bath, maintained at a temperature within 0.3 °C from the freezing point of the reacting solution. This temperature was controlled by recirculation of an antifreeze cooler solution (Halfords Advanced) in a stainless steel coil at the bottom of the bath using a Cole Palmer Polystat® refrigerated chiller. To stop ice formation in the bath, the bath water was enriched with NaCl to near saturation. Exception to this pattern occurred during experiments #3A (first replicate) and #7, when the reacting solution was kept in a separate water bath at 0.8 °C and 25 °C, respectively (Table 1).

Table 1
The composition of stock reacting solution (seawater and seawater-derived brines). All concentrations are reported in μmol kg^{-1} except for Ca^{2+}, which is reported in mmol kg^{-1}. The dry pCO_2 at 1 atm total pressure used to equilibrate the stock reacting solutions prior to the kinetic experiments is in μatm.

Exp	S	t (°C)	SRP	$Si(OH)_4$	A_T	C_T	Ca^{2+}	pCO_2
#1	33.7	−1.1	2.7	22	2277	2213	9.65	389
	33.5	−1.1	4.3	22	2277	2168	9.65	389
#2A	40.0	−2.2	0.0	148	2799	2653	11.56	395
	40.0	−2.2	0.0	148	2799	2638	11.56	395
#2B	40.0	−2.2		148	2799	2645	11.56	395
	40.0	−2.1	0.0	125	2799	2657	11.56	395
[a]#3A	48.8	−2.6	0.0	147	3405	3048	14.08	386
	48.8	−2.6		147	3405	3110	14.08	386
	48.8	−2.6		147	3405	3134	14.08	386
	48.8	−2.6	0.2	183	3478	3173	14.08	408
	48.8	−2.6	0.1	117	3405	3359	14.08	2009
#3B	48.8	−2.6		147	3405	3143	14.08	386
	48.8	−2.6	0.2	147	3478	3144	14.08	386
#3C	48.8	−2.6	0.3	203	3478	3187	14.08	386
#4	58.6	−3.2	0.2	100	4056	3807	16.85	389
#5A	65.7	−3.6		20	4560	3961	19.13	376
	65.7	−3.6	0.2	120	4560	3973	19.13	406
#5B	65.7	−3.6	0.1	45	4560	4461	19.13	2009
#5C	65.7	−3.6		145	4560	3940	19.13	376
#5D	65.7	−3.6	0.1	106	4560	3459	19.13	103
#5E	65.7	−3.6	0.1	107	4560	3459	19.13	103
#5F	65.7	−3.6	0.0	145	4560	3936	19.13	378
	65.7	−3.6	0.1	107	4560	3459	19.13	103
#5G	65.7	−3.6	0.1	50	4560	3898	19.13	390
#6	80.3	−4.4	0.4	76	5690	4694	23.25	389
[b]#7	85.3	−4.9	1.5	55	5897	4128	25.05	393
#8A	101.8	−5.9	0.0	21	7359	5924	29.86	389
#8B	101.8	−5.9	0.0	22	7359	6657	29.86	2009
#8C	101.8	−5.9	0.0	28	7359	6611	29.86	2009
#9A	123.4	−7.5	0.3	93	5894	4628	34.94	406
#9B	123.4	−7.5	0.3	93	5894	4940	34.94	985
#9C	123.4	−7.5	0.3	93	5894	5271	34.94	2009

[a] Brine pre-equilibrated and kept at +0.8 °C during the experiment.
[b] Brine pre-equilibrated and kept at + 24.9 °C during the experiment.

The freezing point of the reacting solution was calculated from the empirical relationship between absolute salinity (S_A, in g kg^{-1}) and temperature (t) of thermally equilibrated seawater and seawater-derived brines with ice ($t \leqslant -1.9$ °C, $S_A \geqslant 34$ g kg^{-1}), as well as hyposaline liquid inclusions ($t > -1.9$ °C, $S_A < 34$ g kg^{-1}) in decaying sea ice, $S_A = 1000\left(1 - \frac{54.11}{t}\right)^{-1}$ (Assur, 1958; Leppäranta and Manninen, 1988; Petrich and Eicken, 2010). Absolute salinity and conductivity-based salinity (practical salinity, S) were related by $S_A = 1.004715\,S$ (Millero and Huang, 2009).

2.2. Steady state assessment

The aim was the determination of the steady state reaction rate, and so, it was desirable to assess the time lag for the attainment of steady state in the concentration changes in the reacting solution during the experiments. Typically, this is achieved non-intrusively by potentiometric monitoring of the change of the solution pH during solid–solution reaction with a glass electrode, to determine a plateau of constant values in the pH time series (Zhong and Mucci, 1993; Zuddas et al., 2003). This was not possible in the salinity and temperature conditions of the current experiments due to lack of suitably characterized pH buffers and the uncertainty about the electrochemical behaviour of the internal electrolyte solution of glass electrodes at sub-zero temperatures. Instead, a time series for the concentration changes in solution during solid–solution reaction was generated by varying the delivery time of a fixed amount of reacting solution (~110 g; see Section 2.1) into the reactor, with each time point being a discrete (complete) experimental run, yielding the full suite of chemical analyses outlined in Section 2.3 below.

2.3. Sampling and analysis

The salinity of the reacting solutions was measured at laboratory temperature (18–26 °C) using a portable conductivity meter (WTW Cond 3110) with a WTW Tetracon 325 probe. When salinities exceeded 70, they were determined following gravimetric dilution with distilled

water. The water bath temperature was recorded every 15 min using data loggers (TINYTAG AQUATIC 2 TG-4100) and also manually twice daily using type K temperature probes on a COMARK 9001 thermometer, with an overall temperature stability as $\pm 1\sigma$ better than 0.1 °C. Samples were taken at the onset of the experimental run from the stock reacting solution and at the end, after the time lag for the attainment of steady state, from the solution in the reactor. The samples were filtered through disposable syringe filters (0.2 μm pore size, 25 mm, WHATMAN GD/X) and were used for the determination of total alkalinity (A_T), C_T, total dissolved calcium (Ca^{2+}), soluble reactive phosphorus (SRP), and molybdenum-reactive silicon [hereafter, silicic acid, $Si(OH)_4$]. The bulk synthetic material used as seed and the solids recovered from precipitation and dissolution experiments were characterized by Synchrotron X-ray Powder Diffraction on the I11 Beam Line at Diamond Light Source (Harwell Science and Innovation Campus, Oxfordshire, UK). Further sampling and analytical detail has been reported in Papadimitriou et al. (2013).

2.4. Determination of the saturation state of ikaite

The degree of saturation (Ω) of aqueous solutions with respect to a $CaCO_3$ polymorph is given by $\Omega = \frac{[Ca^{2+}][CO_3^{2-}]}{K^*_{sp}}$ (Millero, 1995), with quantities in brackets denoting ionic concentrations in mol $kg^{-1}_{solution}$ (hereafter, mol kg^{-1}) and K^*_{sp} = ionic concentration product in solution at equilibrium with the polymorph (stoichiometric equilibrium solubility product, in $mol^2\ kg^{-2}$). The degree of saturation is the driving force for the precipitation of the polymorph from supersaturated solutions ($\Omega > 1$) and, conversely, for its dissolution when in contact with undersaturated solutions ($\Omega < 1$).The determination of the K^*_{sp} of ikaite ($K^*_{sp,ikaite}$) in the same salinity and temperature conditions in parallel seeded closed system experiments has been reported in Papadimitriou et al. (2013). The initial saturation state of the reacting solution ($\Omega^{initial}_{ikaite}$) is required for the modelling of the measured reaction rates. To prevent $CaCO_3$ precipitation in the delivery tubing at low experimental pCO_2 conditions (< 300 μatm), the pCO_2 of the reacting solution entering the reactor was often higher than the reaction pCO_2 (Tables 1 and 2). However, the direction of the reaction (precipitation or dissolution) in the reactor and its extent were driven by the reaction pCO_2. Hence, the initial CO_3^{2-} concentration and $\Omega^{initial}_{ikaite}$ in the reactor were estimated from the measured initial A_T of the reacting solution and the pCO_2 of the reaction for all experiments, coupled with the measured initial Ca^{2+} and the reported $K^*_{sp,ikaite}$ (Table 3). The degree of saturation of the reacting solution with respect to ikaite at the end of each experiment (Ω^{final}_{ikaite}) was computed from the reported $K^*_{sp,ikaite}$, the measured final Ca^{2+}, and the CO_3^{2-} concentration computed from the measured final A_T and C_T (Table 2).

All the above calculations were done by solving for pH the system of equations that describe the CO_2 system of acid-base equilibrium reactions in seawater (DOE, 1994), coupling A_T with C_T or pCO_2 as input parameters, and using the first and second dissociation constants of carbonic acid computed from the salinity and temperature functions derived from the refitting by Dickson and Millero (1987) of the measurements of Mehrbach et al. (1973). The dissociation constants of the remainder of the weak acids and bases pertinent to the oceanic CO_2 system were computed from the equations in Millero (1995) and DOE (1994). The total boron concentration ($[B_T]$), required for the calculation of the contribution of borate alkalinity (A_B) to A_T, was calculated as a linear function of salinity (Millero, 1995) based on $[B_T] = 0.000433$ mol kg^{-1} at $S = 35$ (Lee et al., 2010). Solving the CO_2 system from A_T and pCO_2 also required conversion of dry pCO_2 to wet fCO_2 (fugacity), which was done using the principles and equations in Pierrot et al. (2009). The dissolved CO_2 was then calculated from the computed wet fCO_2 and the CO_2 solubility constant derived from the salinity and temperature function in Weiss (1974). All computations were conducted on the seawater proton scale (SWS) in mol kg^{-1} with the Solver routine on Microsoft Excel after extrapolation of the equations to the experimental salinity and temperature conditions.

The CO_2 system in brine was also modeled using the above routine, to obtain estimates of the modification in the CO_3^{2-} concentration and, from this, the change in Ω_{ikaite} in brine pockets and channels in sea ice. The model results were then combined with the kinetic results in this study, to inform on the time scale of the ikaite–solution reaction in the polar environment. The following scenarios were considered: (i) solving the CO_2 system for pH with conserved surface oceanic Ca^{2+}, A_T, and C_T as input parameters, equivalent to the physical concentration of solutes as a function of brine salinity and, hence, ice temperature; (ii) conserved surface oceanic A_T and Ca^{2+} but non-conservative C_T behaviour by forcing the pCO_2 of the brine to the atmospheric value, equivalent to brine CO_2 degassing to atmospheric equilibrium; and (iii) non-conservative Ca^{2+}, A_T and C_T behaviour, by forcing the pCO_2 and Ω_{ikaite} of the brine to atmospheric and ikaite–brine equilibrium ($\Omega_{ikaite} = 1$), respectively, equivalent to CO_2 degassing and ikaite precipitation from the sea ice brine. In all scenarios, the concentrations of dissolved inorganic nutrients in surface oceanic water were also conserved.

A fixed $pCO_2 = 390$ μatm was used as an input parameter for the atmospheric value in scenarios (ii) and (iii). In scenario (iii), moreover, the system of equations was solved iteratively in two steps; in step 1, the system was solved for brine pH as in scenario (ii) for conservative surface oceanic A_T and atmospheric pCO_2 as input parameters; in step 2, the brine A_T was modified so that the system became saturated with respect to ikaite ($\Omega_{ikaite} = 1$) using the $K^*_{sp,ikaite}$ reported in Papadimitriou et al. (2013) and setting the Ca^{2+} concentration to decline from the conservative value by an amount equivalent to half the change in A_T as per stoichiometry of the ikaite precipitation reaction (see Section 3.1).For the above simulations, the brine salinity was calculated from the empirical relationship between ice temperature and brine S_A mentioned earlier in Section 2.1. Conservative concentrations were computed as linear functions of salinity. The initial input values were the concentrations measured in surface seawater (SSW) from the upper

Table 2
Final measurements: All concentrations are reported in μmol kg^{-1} except for Ca^{2+}, which is reported in mmol kg^{-1}. The $pK^*_{sp,ikaite} = -\log K^*_{sp,ikaite}$ (in $mol^2\ kg^{-2}$) is the average of the reported values per (matching) temperature in Papadimitriou et al. (2013), except for experiments #4 and #6, in which the $K^*_{sp,ikaite}$ was derived from the temperature function in seawater-derived brines at thermal equilibrium with ice in Papadimitriou et al. (2013). The dry pCO_2 at 1 atm total pressure during the kinetic experiments is reported in μatm.

Exp	Reaction time (days)	Reaction	pCO_2	SRP	$Si(OH)_4$	A_T	C_T	[a]$[CO_3^{2-}]_{final}$	Ca^{2+}	$pK^*_{sp,ikaite}$	Ω^{final}_{ikaite}
#1	7	Dissolution	389	9.4	47	5326	4834	410	11.16	5.362	1.1
	5	Dissolution	406	7.3	26	5161	4651	423	11.14		1.1
#2A	5	Dissolution	395	0.0	148	5614	4969	531	12.81	5.233	1.2
	5	Dissolution	395	17.6	158	5360	4801	444	12.97		1.0
#2B	5	Dissolution	99		148	3685	2833	620	12.18		1.3
	7	Dissolution	103	0.1	158	3485	2845	459	12.08		0.9
#3A	5	Dissolution	386		147	5385	4620	601	15.75	5.176	1.4
	5	Dissolution	386		147	5615	4939	542	15.39		1.3
	5	Dissolution	386		147	5428	4760	530	15.34		1.2
	5	Dissolution	408	10.1	198	5381	4654	564	15.04		1.3
	7	Dissolution	389	12.3	148	5328	4620	548	15.25		1.3
#3B	5	Dissolution	97		147	3718	2914	563	14.08		1.2
	7	Dissolution	99	22.5	220	3611	2832	521	14.08		1.1
#3C	5	Precipitation	22	7.8	196	2788	1878	560	13.74		1.2
#4	7	Precipitation	109	13.1	142	3924	3112	548	16.69	5.054	1.0
#5A	5	Dissolution	376	0.4	20	5355	4549	605	19.44	4.981	1.1
	7	Dissolution	406	3.3	142	5323	4547	578	19.39		1.1
#5B	7	Dissolution	298	9.5	85	4940	4196	538	19.17		1.0
#5C	5	Dissolution	244		145	4636	3836	569	19.14		1.0
#5D	7	Precipitation	208	12.2	132	4484	3545	647	19.07		1.2
#5E	7	Precipitation	200	12.3	136	4472	3569	622	19.11		1.1
#5F	5	Precipitation	104		145	3801	2877	605	18.92		1.1
	7	Precipitation	103	12.5	133	3746	2790	613	18.62		1.1
#5G	7	Precipitation	21	3.9	81	3170	2220	572	18.45		1.0
#6	7	Precipitation	99	0.4	76	3951	2936	634	22.28	4.868	1.0
#8A	7	Precipitation	389	8.9	53	5188	4029	738	28.71	4.699	1.1
#8B	7	Precipitation	20	10.5	53	3762	2403	723	27.95		1.0
#8C	7	Precipitation	1014	4.4	51	6878	5913	708	29.58		1.0
#9A	7	Precipitation	406	2.5	113	4869	3795	604	34.73	4.614	0.9
#9B	7	Dissolution	985	3.4	111	6310	5174	729	34.83		1.0
#9C	7	Dissolution	2009	3.5	110	8007	6957	766	35.70		1.1

[a] Calculated from the measured final C_T and A_T.

100 m of the Weddell Sea, Antarctica, in early spring 2006, normalized to S = 35 (Papadimitriou et al., 2012): $[SRP]_{SSW} = 2.11$ μmol kg^{-1}, $[Si(OH)_4] = 68$ μmol kg^{-1}, $[NH_4^+] < 0.05$ μmol kg^{-1}, $[C_T]_{SSW} = 2262$ μmol kg^{-1}, $[A_T]_{SSW} = 2369$ μmolkg^{-1}, with $[Ca^{2+}]_{SSW} = 0.01028$ mol kg^{-1}. With these input parameters and conforming to the existing empirical data set for $K^*_{sp,ikaite}$ in seawater, the model yielded $pH_{SWS} = 8.017$, $CO_2(aq) = 28.0$ μmol kg^{-1}, $[CO_3^{2-}] = 85$ μmol kg^{-1}, $fCO_2 = 413$ μatm, and $\Omega_{ikaite} = 0.17$ at −1.9 °C (freezing point at S = 35) and $pH_{SWS} = 8.004$, $CO_2(aq) = 28.2$ μmol kg^{-1}, $[CO_3^{2-}] = 85$ μmol kg^{-1}, $fCO_2 = 429$ μatm, and $\Omega_{ikaite} = 0.20$ at −1.1 °C.

2.5. Determination of the reaction rate

The net reaction (dissolution or precipitation) rate was computed from the difference between initial and final A_T ($A_{T,o}$ and $A_{T,final}$, respectively, in μmol kg^{-1}) during the experimental time course (Δt, in h), and the stoichiometric molar ΔA_T to ikaite ratio of 2 (see equilibrium reaction in Section 3.1) as (i) bulk solution rate, $R_{bulk\text{-}sln} = \frac{[A_{T,final}]-[A_{T,0}]}{2\Delta t}$ (in μmol $kg^{-1}_{solution}$ h^{-1}), (ii) rate normalized to the mass of the synthetic ikaite seed (m_{seed}), $R_{mass} = J\frac{[A_{T,final}]-[A_{T,0}]}{2\ m_{seed}}$ (in μmol g^{-1}_{seed} h^{-1}), and (iii) rate normalized to both mass and the estimated surface area of the synthetic ikaite seed, $R_{SA} = J\frac{[A_{T,final}]-[A_{T,0}]}{2\ SA\ m_{seed}}$ (in μmol m^{-2}_{seed} h^{-1}). In the above equations, J is the delivery rate of the reacting solution over the minimum of 5 days of reaction required for the achievement of steady state (0.94 ± 0.01 g h^{-1}, n = 13; see Section 3.1) and SA is the geometric surface area of the synthetic ikaite seed (0.021 ± 0.010 m^2 g^{-1}; Papadimitriou et al., 2013). Because ikaite dissolution leads to a total alkalinity increase in solution, and vice versa during precipitation, the dissolution rates were computed and are given as positive numbers and the precipitation rates as negative.

In this study, $R_{bulk\text{-}sln}$ was used in the simple modelling of ikaite in sea ice outlined in the previous section. The rate expressed as R_{mass} is relevant to natural settings because it is the mass rather than the surface area of ikaite that has been measured in most field studies (Dieckmann et al., 2008; Fischer et al., 2013; Rysgaard et al., 2013). Finally, R_{SA} conforms to the literature of $CaCO_3$ kinetic studies. Hence, the ikaite kinetic rates are presented and discussed

Table 3
Ikaite precipitation and dissolution rates. Precipitation is indicated by negative sign. The $R_{bulk\text{-}sln}$ is given in μmol $kg^{-1}_{solution}$ h^{-1}, R_{mass} in μmol g^{-1}_{seed} h^{-1}, and the R_{SA} in μmol m^{-2}_{seed} h^{-1}.

Exp	Reaction	[a]$[CO_3^{2-}]_{initial}$	[b]$\Omega^{initial}_{ikaite}$	$R_{bulk\ sln}$	R_{mass}	R_{SA}
#1	Dissolution	85	0.189	9.1	4.73	227
	Dissolution	82	0.181	12.1	4.31	207
#2A	Dissolution	130	0.257	12.0	4.39	210
	Dissolution	130	0.257	10.9	3.92	188
#2B	Dissolution	329	0.650	3.8	1.37	66
	Dissolution	323	0.638	2.0	1.06	51
#3A	Dissolution	212	0.448	8.4	3.07	147
	Dissolution	212	0.448	9.4	3.42	164
	Dissolution	212	0.448	8.6	3.15	151
	Dissolution	211	0.446	8.1	3.05	146
	Dissolution	211	0.445	5.7	2.98	143
#3B	Dissolution	489	1.032	1.3	0.49	23
	Dissolution	500	1.057	0.4	0.21	10
#3C	Precipitation	848	1.792	−2.9	−1.09	−52
#4	Precipitation	651	1.242	−0.4	−0.20	−10
#5A	Dissolution	435	0.797	3.4	1.22	58
	Dissolution	414	0.759	2.3	1.17	56
#5B	Dissolution	500	0.916	1.1	0.59	28
#5C	Dissolution	559	1.024	0.3	0.12	6
#5D	Precipitation	608	1.113	−0.2	−0.12	−6
#5E	Precipitation	620	1.135	−0.3	−0.14	−7
#5F	Precipitation	827	1.515	−3.2	−1.18	−57
	Precipitation	831	1.522	−2.4	−1.24	−60
#5G	Precipitation	1290	2.363	−4.1	−2.16	−104
#6	Precipitation	1247	2.141	−5.2	−2.66	−127
#8A	Precipitation	1230	1.837	−6.5	−3.34	−160
#8B	Precipitation	2467	3.685	−10.7	−5.63	−270
#8C	Precipitation	751	1.121	−1.4	−0.73	−35
#9A	Precipitation	960	1.378	−3.0	−1.59	−76
#9B	Dissolution	633	0.908	1.2	0.65	31
#9C	Dissolution	406	0.583	6.3	3.28	157

[a] Computed from the measured initial [A_T] (see Table 1) and reaction pCO_2 (see Table 2).
[b] Computed from $[CO_3^{2-}]_{initial}$, the measured initial [Ca^{2+}] (see Table 1), and the $K^*_{sp,ikaite}$ from Papadimitriou et al. (2013) (see Table 2).

as R_{SA} in Sections 4.1 and 4.2, while $R_{bulk\text{-}sln}$ is used in Section 4.3. In both cases, linear regression was used based on the Geometric Mean Regression theory (Ricker, 1973). Changes in the surface area of the solids during the reaction were neglected because, based on the measured A_T changes, the reaction resulted in solid mass changes equivalent to less than 12% and 14% of the seed mass during dissolution and precipitation, respectively.

3. RESULTS

Bulk seed and solids recovered after the reaction experiments were identified as ikaite by X-ray powder diffraction, which indicates that ikaite was the only salt present in the solid phase during the kinetic experiments of this study. The average (±1σ) initial Ca^{2+} concentration in the brines (Table 1), normalized to a salinity of 35 (10.17 ± 0.08 mmol kg^{-1}, n = 7) was comparable to the equivalent concentration in the parent seawater (10.13 ± 0.12 mmol kg^{-1} at S = 35; Papadimitriou et al., 2013) in all but the brine used for experiment #9, in which the salinity-normalized Ca^{2+} concentration was 9.91 mmol kg^{-1}. This indicates that in all brine batches, except that used for experiment #9, there was no measurable loss of Ca^{2+} to $CaCO_3$ or $CaSO_4$ polymorphs during brine preparation by seawater freezing. The brine used for experiment #9 also had a (salinity-normalized) A_T deficit relative to the remainder of the brine batches, which suggests that the Ca^{2+} deficit in this brine batch was lost to $CaCO_3$ precipitation during preparation. Nonetheless, these deficits affect the carbonate ion concentration and the initial saturation state of the brine with respect to ikaite rather than the reaction mechanism. Hence, experiment #9 was considered to provide useful information on the reaction kinetics of ikaite at the maximum salinity and minimum temperature conditions of this study and was taken into account.

3.1. Time series: steady state assessment

The time required for the concentration changes resulting from the ikaite–solution reaction to reach steady state in the experimental conditions of the study was evaluated from undersaturation in seawater in experiment #1 (S = 34, t = −1.1 °C, reaction pCO_2 = 389 and 406 μatm) and in brine in experiment #3 (S = 49, t = −2.6 °C, reaction pCO_2 = 389 and 408 μatm), and from supersaturation in brine during experiment #7 (S = 85, t = −4.9 °C, reaction pCO_2 = 22 μatm) (Fig. 1). All concentration changes

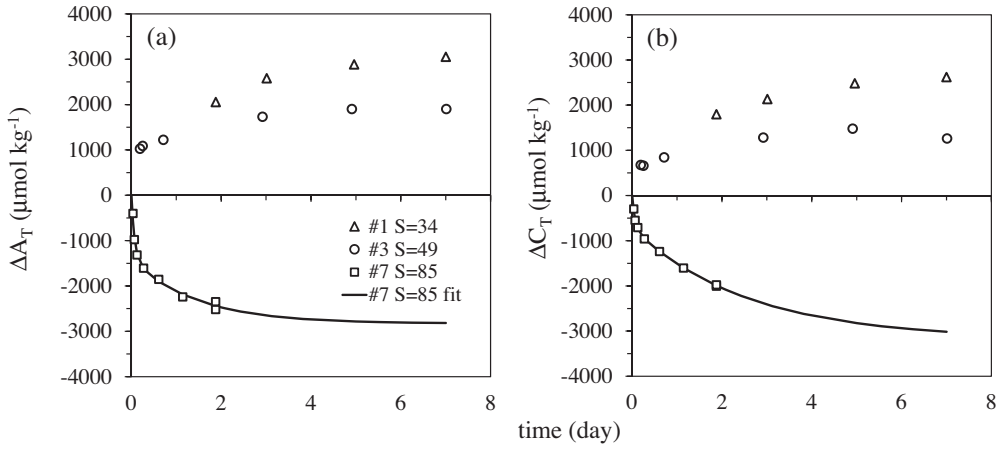

Fig. 1. The change in (a) total alkalinity and (b) total dissolved inorganic carbon as a function of solid–solution reaction time.

measured during the time series experiments were commensurate with the equilibrium ikaite–solution reaction in an open system, $2HCO_3^- + Ca^{2+} + 5H_2O \leftrightarrow CaCO_3 \cdot 6H_2O + CO_2 \uparrow$, with stoichiometric molar ratios of ΔA_T: ΔC_T = 1:1 and ΔA_T: ΔCa^{2+} = ΔC_T: ΔCa^{2+} = 2:1 (Fig. 2). The time series from undersaturation (ikaite dissolution) in both seawater and brine (experiments #1 and #3; Fig. 1) indicated attainment of stable concentration (i.e., the concentration change was within the analytical and experimental variability; see next Section) after 5 days of reaction, which is commensurate with the two-week long minimum equilibration times required in closed system experiments (changing pCO_2) as reported in Papadimitriou et al. (2013). This was also evident in experiment #7 (ikaite precipitation), when the monitored 2 days of the precipitation reaction from supersaturation were not sufficient for the concentration changes to reach steady state (Fig. 1). Hence, experiment #7 was not used for reaction rate determination. However, the A_T changes observed during experiment #7 were fitted best to an empirical double exponential function of time with the boundary conditions of $[A_T] = [A_T]_o$ at $t = 0$ and $[A_T] = [A_T]_{ss}$ (steady state A_T) at $t \rightarrow \infty$, yielding $\Delta A_T = [A_T] - [A_T]_o = ([A_T]_{ss} - [A_T]_o)\ (1 - e^{-b_1 t}) - a_2\ (e^{-b_1 t} - e^{-b_2 t})$, with t = time (d) and a_2 = fitted constant. Minimizing the sum of squared residuals with the Solver routine in Excel gave $\Delta A_T = -2829\ (1 - e^{-0.69 t}) - 1426\ (e^{-0.69 t} - e^{-13.26 t})$ ($r^2 = 0.831$, $p < 0.001$, $n = 8$) (Fig. 1a). The observed C_T changes during experiment #7 were also fitted to a similar empirical function of time, yielding $\Delta C_T = [C_T] - [C_T]_o = -3177\ (1 - e^{-0.39 t}) - 725\ (e^{-0.39 t} - e^{-14.81 t})$ ($r^2 = 0.833$, $p < 0.001$, $n = 8$) (Fig. 1b). This simple empirical model indicated that, under the conditions of experiment #7, achievement of the equivalent of ⩾98% of the steady state concentration change would require ⩾5 days of reaction for a total reacting solution of about 110 g in the reactor. Hence, all ensuing experiments were

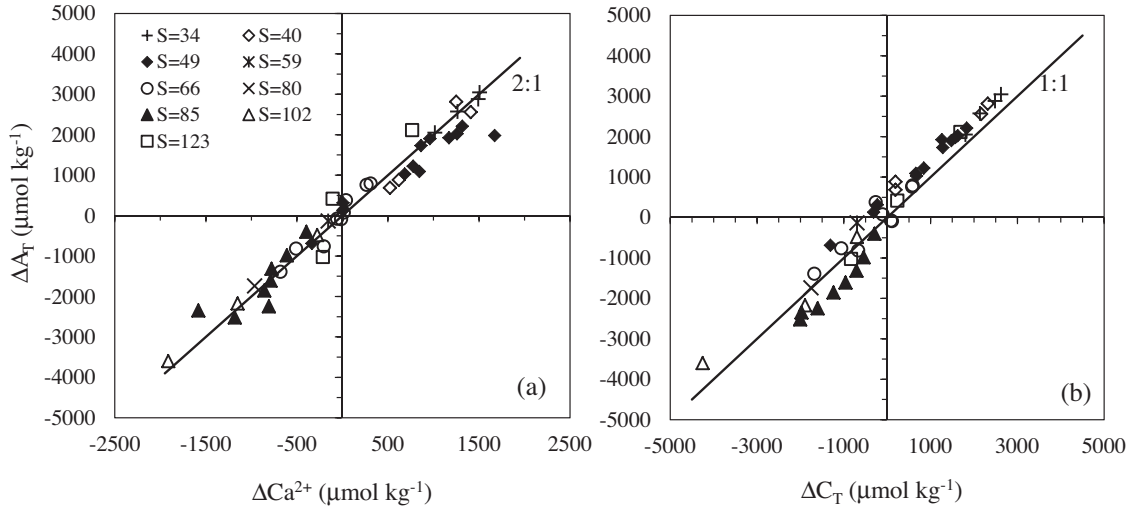

Fig. 2. The change in total alkalinity as a function of the concentration change in (a) dissolved calcium, and (b) total dissolved inorganic carbon. The straight line in panels (a) and (b) has a slope equivalent to the corresponding stoichiometric molar ratio of the $CaCO_3$-solution reaction in an open system.

conducted for 5 or 7 days, with a solution delivery rate of 0.94 ± 0.01 g hr^{-1} ($n = 13$) and 0.69 ± 0.05 g hr^{-1} ($n = 18$), respectively, and all reaction rates were computed from the measured A_T change for the minimum of 5 days of reaction.

3.2. Reaction kinetics of ikaite at sub-zero temperatures

A total of 31 seeded experiments were conducted for the investigation of the reaction rate of ikaite precipitation and dissolution at sub-zero temperatures in high ionic strength natural solutions (Tables 1 and 2). Detailed information on the estimated $\Omega_{ikaite}^{initial}$ and the measured reaction rates is given in Table 3. All concentration changes were commensurate with the equilibrium $CaCO_3$-solution interaction in an open system as described in Section 3.1 (Fig. 2). The replication of several experiments, i.e., #1, #2A, #2B, #3B, #5A, and #5F ($n = 2$), as well as #3A ($n = 5$), yielded an estimate of the combined analytical and experimental variability of the final A_T concentration (Table 2), on which the reaction rate is based. Expressed as range of the final measurements per experiment, the combined analytical and experimental variability ranged from 32 to 287 μmol kg^{-1}, equivalent to 0.6–6% of the average final A_T at $[A_T] \approx 3500$–5500 μmol kg^{-1}. The attendant uncertainty in the reaction rate (Table 3) was better than 26%, except for the very low dissolution rates in experiment #3B, where it was 81%.Overall, the direction of the reaction was effectively controlled by the pCO_2 in the reactor. The estimated $\Omega_{ikaite}^{initial}$ ranged from 1.02 to 3.69 in conditions of supersaturation with respect to ikaite ($n = 15$) and from 0.18 to 0.92 in conditions of undersaturation ($n = 16$) (Table 3). An uncertainty in $\Omega_{ikaite}^{initial}$ of up to 0.03 Ω-units was due to the analytical uncertainty in the initial Ca^{2+} concentration (0.2–2.0%; Papadimitriou et al., 2013). Additional uncertainty in $\Omega_{ikaite}^{initial}$ was incurred by the indeterminable computational uncertainty in the initial CO_3^{2-} concentration from the extrapolation of the salinity and temperature functions that describe the oceanic CO_2 system to the sub-zero temperatures and high salinities of the experiments. The overall uncertainty is particularly evident in reaction conditions very close to equilibrium from the direction of supersaturation in experiments #3B ($\Omega_{ikaite}^{initial} = 1.03$ and 1.06; $n = 2$) and #5C ($\Omega_{ikaite}^{initial} = 1.02$). In those experiments, the calculated $\Omega_{ikaite}^{initial}$ indicated slight supersaturation, while the observed final ΔA_T indicated ikaite dissolution (positive rate; Table 3), suggesting slight undersaturation. Thus, supersaturation conditions within less than 0.1 units from $\Omega = 1$ cannot be resolved with the current combined analytical, experimental, and computational uncertainty, and will not be taken into further consideration.

4. DISCUSSION

4.1. The empirical rate law of ikaite precipitation and dissolution

The kinetics of the precipitation and dissolution of the anhydrous $CaCO_3$ polymorphs calcite and aragonite, determined as bulk rate from changes in solution composition, have been typically related to the saturation state of the solution with respect to these polymorphs as $R_{ppt} = k_{ppt}(\Omega - 1)^n$ and $R_{diss} = k_{diss}(1 - \Omega)^n$, respectively (Zhong and Mucci, 1993; Morse et al., 2007). In these empirical rate laws, k = reaction rate constant (in μmol m^{-2} h^{-1}) and n = reaction order, while the functions are linearized by logarithmic transformation. Although not suitable for assessment of solid–solution reaction mechanisms at the microscopic level, the empirical rate laws have been useful in environmental applications to both dilute and highly concentrated electrolyte solutions, such as seawater and brines. The current observations of the surface-area-normalized ikaite precipitation rate (R_{SA}) yielded $n = 1.23 \pm 0.42$ and $\log k_{ppt} = 2.07 \pm 0.23$ within $1.1 \leqslant \Omega_{ikaite}^{initial} \leqslant 3.7$ ($r^2 = 0.742$, $p < 0.001$, $n = 12$; Fig. 3a). The equivalent analysis for the ikaite dissolution rate yielded $n = 0.98 \pm 0.18$ and $\log k_{diss} = 2.41 \pm 0.09$ within $0.2 \leqslant \Omega_{ikaite}^{initial} \leqslant 0.9$ ($r^2 = 0.888$, $p < 0.001$, $n = 16$; Fig. 3b).

The current measurements are the first set of observations for the ikaite reaction kinetics in natural waters. To place them in the broader context of metal carbonate reaction kinetics in the aquatic environment, the current observations can be compared tentatively to the more widely available equivalent kinetic rate observations for calcite and aragonite. The literature data have been derived either in synthetic seawater or in compositionally simpler NaCl–$NaHCO_3$–$CaCl_2$ solutions of ionic strength ranging from the dilute (<0.1 m) to the highly concentrated (ionic strength ⩾0.7 m). Given the ionic complexity of the current media, our primary comparison will be with kinetic data obtained from the reaction of anhydrous $CaCO_3$ polymorphs with synthetic seawater. This comparison shows that the reaction order of ikaite precipitation ($n = 1.23 \pm 0.42$) at sub-zero temperatures is comparable to – but closer to first order reaction kinetics than – that of calcite precipitation at 5 °C ($n = 1.55 \pm 0.17$) and 25 °C ($n = 1.84 \pm 0.20$ and 2.22 ± 0.05) (Zhong and Mucci, 1993; Lopez et al., 2009) and aragonite precipitation at 25 °C ($n = 1.90 \pm 0.10$; Burton and Walter, 1987). Moreover, the ikaite precipitation rate in the current hypersaline and sub-zero temperature conditions close to saturation (i.e., $\Omega_{ikaite}^{initial} \leqslant 3.7$) was higher than the reported calcite precipitation kinetics at above-zero temperatures in the Ω range of this study, being as high as aragonite precipitation kinetics in seawater at 25 °C. The comparison extends to the saturation conditions, although the precipitation kinetics of the anhydrous $CaCO_3$ polymorphs was also measured at much higher supersaturation than that of ikaite in the present study (Fig. 3a). The above comparison becomes more evident in terms of the reaction rate constant for ikaite precipitation ($\log k_{ppt} = 2.07 \pm 0.23$), which was similar to that for aragonite in seawater at 25 °C ($\log k_{ppt} = 1.61 \pm 0.01$; Burton and Walter, 1987) but higher, by an order of magnitude, than that reported for calcite in much warmer seawater, i.e., $\log k_{ppt} = 0.20 \pm 0.04$ at 5 °C, and 0.33 ± 0.05 and 0.21 ± 0.13 at 25 °C (Zhong and Mucci, 1993; Lopez et al., 2009). The precipitation rate of calcite has been reported to decline by a similar amount in the presence of ionic inhibitors in the composition of seawater (e.g., magnesium and sulphate ions, orthophosphate)

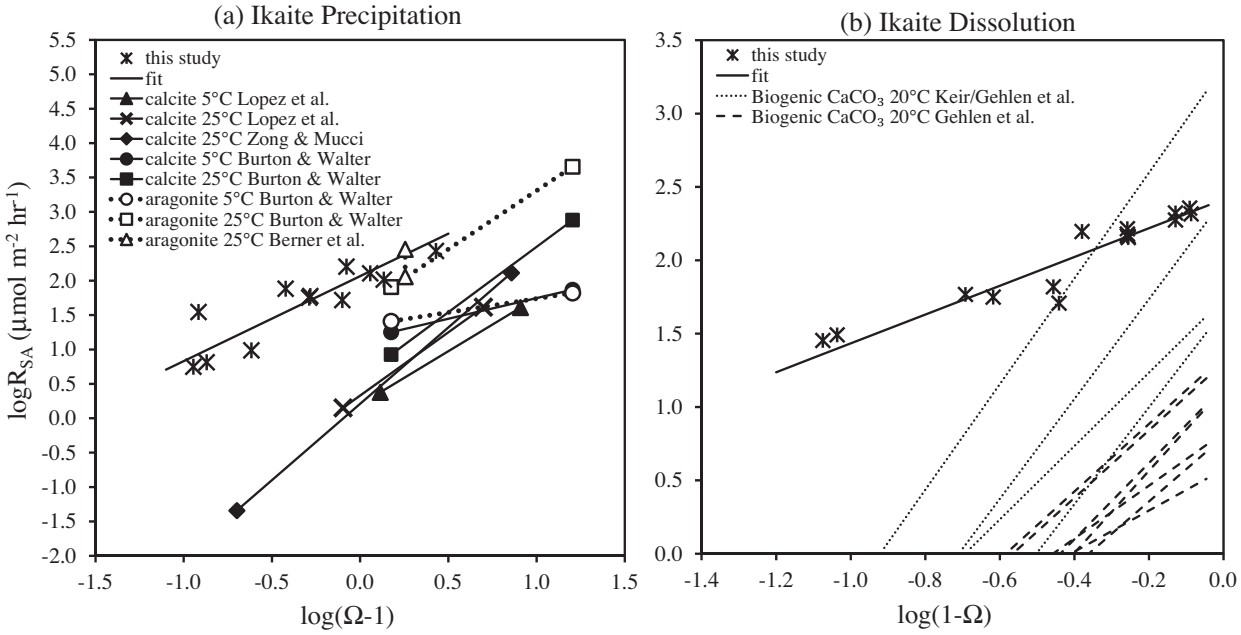

Fig. 3. Logarithm of the surface-area-normalized ikaite-solution reaction rate as a function of the logarithm of the deviation of the saturation state of the solution from equilibrium with respect to ikaite. The empirical rate law for calcite and aragonite precipitation is plotted in panel (a) across the range of the initial saturation state in experiments at above-zero temperatures in artificial seawater, taken from Berner et al. (1978), Burton and Walter (1987), Zhong and Mucci (1993), and Lopez et al. (2009). The empirical rate law for calcite and aragonite dissolution is plotted in (b) from dissolution experiments with marine biogenic (foraminifera and sedimentary) $CaCO_3$ at 20 °C in artificial seawater reported in Gehlen et al. (2005).

(Busenberg and Plummer, 1985; Bischoff et al., 1993; Davies et al., 2000; Hu et al., 2014).

In contrast, the observed dissolution kinetics of ikaite differed substantially from that of synthetic and biogenic calcite, low Mg calcite, and aragonite (Fig. 3b). The current observations yielded first order dissolution kinetics for ikaite ($n = 0.98 \pm 0.18$), which is distinctly different from the second to fourth order reported for the dissolution reaction of the anhydrous $CaCO_3$ polymorphs in seawater at 20 °C (Gehlen et al., 2005). Furthermore, the reaction rate constant for ikaite dissolution ($\log k_{diss} = 2.41 \pm 0.09$) was larger than that for sedimentary biogenic calcite and aragonite explored for their dissolution kinetics in warm synthetic seawater in Gehlen et al. (2005) ($\log k_{diss} = 0.57 - 1.30$, after unit conversion). It appears, therefore, that the ikaite dissolution rate in cold seawater and seawater-derived brines is much higher than that of calcite and aragonite in warm seawater.

4.2. The effect of ionic strength and temperature

Temperature variation affects solid–solution reaction kinetics via the temperature effect on the reaction rate constant (Morse et al., 2007). In addition, both the stoichiometric solubility of ikaite and the equilibrium speciation of dissolved CO_2 will be affected by the temperature of the solid–solution reaction and the ionic strength of the medium (Mucci, 1983; DOE, 1994; Millero, 1995; Papadimitriou et al., 2013). The temperature–salinity–pCO_2 conditions of the current experiments were chosen to reflect the temperature–salinity co-variation of thermally equilibrated sea ice brines (Assur, 1958) and the lower part of the pCO_2 range reported in sea ice to values well below atmospheric equilibrium (Gleitz et al., 1995; Delille et al., 2007; Papadimitriou et al., 2007). Such low pCO_2 is, evidently, most favourable to ikaite precipitation (Papadimitriou et al., 2013) and, consequently, to its investigation.

The influence of ionic strength on metal carbonate reaction kinetics has been investigated in a limited number of studies of calcite reaction kinetics in highly concentrated (ionic strength > 0.7 m) simple electrolyte solutions (NaCl) at above-zero temperatures (Zuddas and Mucci, 1998; Gledhill and Morse, 2006; Finneran and Morse, 2009). These studies have shown an ionic strength (salinity) dependency of the reaction rate of calcite precipitation and dissolution. Specifically, the precipitation rate of calcite has been found to increase with increasing ionic strength (at constant temperature and pCO_2) (Zuddas and Mucci, 1998). As outlined above, the current experimental design cannot yield information that would allow separation of the effect of ionic strength (at constant temperature) from the temperature effect (at constant ionic strength) on the reaction rate of ikaite as a function of solution saturation. The variation of pCO_2 conditions at constant salinity and temperature yielded limited information on the combined effect of these two physical parameters when coupled in the ice–brine system on the surface of the polar oceans. Sufficient data for statistically significant functions (at better than 90% significance level) of $\log R_{SA}$ versus $\log(\Omega - 1)$ at individual salinity–temperature settings were acquired only at

$S = 65.7$ and $t = -3.6$ °C ($r^2 = 0.939$, $p = 0.004$, $n = 5$) within $1.1 \leqslant \Omega \leqslant 2.4$, and at $S = 101.8$ and $t = -5.9$ °C ($r^2 = 0.965$, $p = 0.085$, $n = 3$) within $1.1 \leqslant \Omega \leqslant 3.7$. This analysis yielded a lower reaction order at $S = 101.8$ and $t = -5.9$ °C ($n = 0.68 \pm 1.14$) than at $S = 65.7$ and $t = -3.6$ °C ($n = 1.31 \pm 0.52$) but a similar reaction rate constant in both cases ($\log k_{ppt} = 2.01 \pm 0.31$ at $S = 65.7$ and $t = -3.6$ °C; $\log k_{ppt} = 2.19 \pm 1.20$ at $S = 101.8$ and $t = -5.9$ °C). The latter is evident in the convergence of both trends at $\log(\Omega - 1) = 0$ ($\Omega = 2$) (Fig. 4); beyond this point, i.e., $\Omega > 2$, a change of slope (i.e., reaction order) of the $CaCO_3$ precipitation function of logR versus $\log(\Omega - 1)$ has been seen for calcite in seawater at 25 °C (Zhong and Mucci, 1993). The above suggest that, in addition to the Ω_{ikaite} of the brine, the salinity and temperature of the ice–brine system appear to exert control on ikaite precipitation kinetics in sea ice via a change in the reaction order in the disequilibrium region close to saturation. The fitted function on all available data reported in Section 4.1 (Fig. 3a) should nevertheless provide a good approximation of the precipitation rate of ikaite within the experimental Ω_{ikaite} range in sea ice brines.

The ionic strength of the solution has been found to have the reverse effect on the dissolution rate of calcite, but the drop in the dissolution rate of calcite with increasing ionic strength was not evident at $pCO_2 < 0.1$ atm (Gledhill and Morse, 2006; Finneran and Morse, 2009). A minimal effect of ionic strength is, therefore, expected on the dissolution rate of ikaite at the much lower pCO_2 conditions during ikaite dissolution of this study. This is implied in the comparatively tight distribution of the current observations around the linear function of $\log(1 - \Omega)$ (Fig. 3b), suggesting that the saturation state of the seawater or brine with respect to ikaite and, by extension, the pCO_2 of the system should be the main controlling parameter of the dissolution rate of this polymorph.

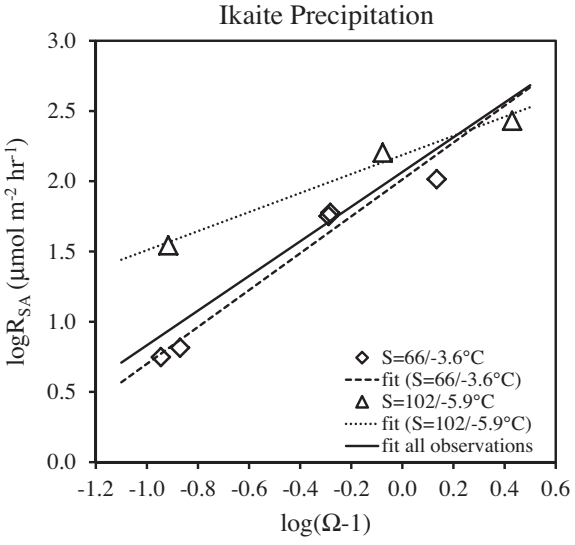

Fig. 4. Logarithm of the surface-area-normalized ikaite-solution reaction rate as a function of the logarithm of the deviation of the saturation state of the solution from equilibrium with respect to ikaite. The solid line for the overall fit is also shown in Fig. 3a.

Finally, the derivation of a rate law from bulk kinetic observations is affected by how well the stoichiometric equilibrium solubility of the solid phase is known, along with the stoichiometric equilibrium constants that describe the equilibrium reactions amongst gaseous CO_2 and aqueous CO_2 species (Hales and Emerson, 1997). The stoichiometric solubility of ikaite (Table 2) has been concurrently measured in the same solutions during long-term closed system incubations as reported in Papadimitriou et al. (2013), but the equilibrium constants that regulate the oceanic CO_2 system are not known from observation in the sub-zero hypersaline conditions of this study; only extrapolation from the fitted observations in the standard oceanic salinity and above-zero temperature range is available to date. The error incurred by the extrapolation is unknown. It is with this caveat that the empirical rate law for ikaite dissolution and precipitation in seawater-derived brines at sub-zero temperatures was obtained and was discussed here across the entire experimental temperature-salinity range.

4.3. Implications for the ikaite cycle in sea ice

With the above stipulation in mind, an attempt will be made below to estimate the time scale of the ikaite–solution reaction in the polar environment by coupling the empirical rate law with the simple model of the brine CO_2 system described in Section 2.4. In the absence of gas exchange, solid–solution reaction, and biological activity during sea ice formation and growth, the physical concentration of the seawater solutes into brine in a closed system leads to conservation of the surface oceanic A_T and C_T in the brine channels and pores of sea ice. This will result in the rise of brine pCO_2 to values more than an order of magnitude higher than the current atmospheric concentration (Table 4). In defence of this result, a commensurate trend has been observed in artificial sea ice (Geilfus et al., 2012), and values as high as 12,000 μatm have been documented in winter sea ice (Miller et al., 2011a,b). Under these elevated pCO_2 conditions, the physical-concentration-driven rise in CO_3^{2-} (Table 4) and Ca^{2+} is insufficient relative to the empirical $K^*_{sp,ikaite}$ for the brine to become saturated with respect to ikaite and, thus, viable for ikaite precipitation in the temperature range from the freezing point of seawater down to −8 °C. In other words, the brine remains corrosive to ikaite (Table 4; $\Omega_{ikaite} < 1.0$).

The increase in brine pCO_2 during the physical concentration of seawater solutes generates a gas–liquid CO_2 disequilibrium, a driver of potential CO_2 escape from the brine into gas bubbles. Brine degassing during wintertime cooling and inorganic carbon uptake by the sympagic autotrophs in the productive layers of sea ice in the spring–summer season are two mechanisms which can depress the brine pCO_2 (Gleitz et al., 1995; Papadimitriou et al., 2007, 2012; Delille et al. 2007; Munro et al., 2010). The lowering of brine pCO_2 will result in re-equilibration of the brine CO_2 system, which yields higher pH and CO_3^{2-} concentration in the brine than the values derived from physical sea salt concentration alone (Table 4). This, in turn, will result in

Table 4
Estimates of parameters of the brine CO_2 system during sea ice cooling based on the model outlined in Section 2.4 for (i) conserved surface oceanic A_T and C_T, (ii) conserved A_T and non-conservative C_T via brine CO_2 degassing to atmospheric equilibrium (atmospheric $pCO_2 = 390$ μatm), and (iii) non-conservative A_T and C_T behaviour via ikaite precipitation to solid–solution equilibrium and CO_2 degassing to atmospheric equilibrium. Solute [including pH on the seawater scale (pH_{SWS})] and ikaite concentrations are given on a per unit brine mass basis as μmol kg^{-1}, while the fugacity of CO_2 (fCO_2) is in μatm. The $pK^*_{sp,ikaite} = -\log K^*_{sp,ikaite}$ (in $mol^2\,kg^{-2}$) was derived from the temperature function in seawater-derived brines at thermal equilibrium with ice in Papadimitriou et al. (2013). The bulk solution precipitation rate of ikaite ($R_{bulk\text{-}sln}$) is in μmol $kg^{-1}_{solution}\,h^{-1}$. The reaction time to ikaite–brine equilibrium (τ) is in days.

Case	S	t	A_T	C_T	pH_{SWS}	CO_3^{2-}	fCO_2	Ikaite $= \Delta Ca^{2+} = \frac{\Delta A_T}{2}$	$pK^*_{sp,ikaite}$	Ω_{ikaite}	$R_{bulk\text{-}sln}$	$\tau = \frac{\Delta A_T/2}{24 R_{bulk\text{-}sln}}$
Conserved	84	−5	5699	5441	7.96	252	1841		4.793	0.39		
CO_2 equilibrium			5699	4684	8.53	721	387			1.11	0.3	22
CO_2 and Ikaite equilibrium			5375	4436	8.51	655	387	162		1.00		
Conserved	99	−6	6725	6420	8.05	311	2655		4.697	0.45		
CO_2 equilibrium			6725	5240	8.73	1045	387			1.52	2.2	14
CO_2 and Ikaite equilibrium			5252	4160	8.65	707	387	737		1.00		
Conserved	114	−7	7718	7368	8.19	371	3702		4.633	0.53		
CO_2 equilibrium			7718	5697	8.97	1401	387			2.01	5.1	11
CO_2 and Ikaite equilibrium			5049	3820	8.83	724	387	1334		1.00		
Conserved	128	−8	8678	8285	8.37	431	5026		4.602	0.65		
CO_2 equilibrium			8678	6073	9.23	1772	387			2.67	9.5	9
CO_2 and Ikaite equilibrium			4754	3413	9.03	701	387	1962		1.00		

conditions favourable for the precipitation of ikaite at the temperature where the solubility of the polymorph is exceeded ($\Omega_{ikaite} > 1.0$). For example, the brine (derived from the surface seawater composition outlined in Section 2.4) at thermal equilibrium with ice at −4.7 °C (S = 79.5) will reach saturation with respect to ($\Omega_{ikaite} = 1.0$) after its pCO_2 has been lowered from the conserved value to atmospheric equilibrium (ca. 390 μatm; Papadimitriou et al., 2013). When the brine cools to temperatures below this onset temperature and, thus, becomes more concentrated but retains its equilibrium with atmospheric pCO_2, the Ω_{ikaite} will rise further to values as high as 2.7 at −8 °C (Table 4).

The above analysis shows that, at best, conserved A_T and non-conserved C_T through the lowering of brine pCO_2 to atmospheric equilibrium will afford modest values for Ω_{ikaite} within the sea ice system (i.e., $\Omega_{ikaite} = 1$–3) in the temperature range from −2 °C to −8 °C (Table 4). This extent of ikaite supersaturation in brines and, in the absence of information for the surface area of authigenic ikaite particles, the bulk solution reaction rate ($R_{bulk\text{-}sln}$; see Section 2.5 for definition; Table 3) will be used here, to compute an estimate of the time scale of ikaite formation in sea ice. The $R_{bulk\text{-}sln}$ was fitted to the same empirical function as R_{SA} (see Section 4.1), yielding, $\log R_{bulk\text{-}sln} = 0.70 + 1.25\ \log(\Omega - 1)$ for the precipitation reaction ($r^2 = 0.746$, $p < 0.001$, $n = 12$) and $\log R_{bulk\text{-}sln} = 1.16 + 1.12\ \log(1 - \Omega)$ for the dissolution reaction ($r^2 = 0.865$, $p < 0.001$, $n = 16$). The steady state reaction rates from the current experiments suggest that the time scale for the ikaite precipitation reaction to reach equilibrium in sea ice is in the order of 1–3 weeks (Table 4), similar to the time frame documented as ikaite occurrence from onset of seawater freezing in young sea ice in field studies (Rysgaard et al., 2012, 2013). The observed dissolution rates imply that, in the severely corrosive conditions of polar surface oceanic seawater (see Section 2.4), ikaite will dissolve at a rate of 281 μmol $kg^{-1}\,d^{-1}$, equivalent to 0.059 g ikaite $kg^{-1}\,d^{-1}$. An area-weighted estimate for the sea ice ikaite content of 0.3–3.0 g m^{-2} was derived from field observations in the Weddell Sea (Dieckmann et al., 2008). Using the dissolution rate above, the reported ikaite content of sea ice will dissolve in a time frame ranging from a few hours to a few days in the surface ocean, assuming that it escapes dissolution during sea ice decay and melt, and is homogeneously mixed throughout a surface mixed layer of 10–50 m thickness.

5. CONCLUSIONS

The precipitation and dissolution rates of ikaite in seawater and seawater-derived brines at sub-zero temperatures were found to conform to the same empirical rate law as those of the anhydrous $CaCO_3$ polymorphs, calcite and aragonite. The reaction order with respect to the deviation of the solution from ikaite saturation was close to first order reaction kinetics, while the reaction rate constant was higher than that of the anhydrous polymorphs. In addition to the saturation state of the brine with respect to ikaite, the salinity and temperature of the brine appear to exert control on ikaite precipitation kinetics, while the dissolution kinetics of the polymorph appear impervious to their influence.

Simple modelling of the brine CO_2 system demonstrated that the physical concentration of seawater solutes coupled with the changes in ikaite solubility in the temperature and salinity conditions of sea ice formation and growth to −8 °C are insufficient to drive the internal sea ice brines to ikaite precipitation. The loss of dissolved inorganic carbon to the gas phase of sea ice and, with potentially more dramatic results, to the sympagic autotrophic community can be a potent trigger of the ikaite cycle via regulation of the brine pH and, with it, the carbonate ion concentration in the brine through the C_T species re-equilibration.

Based on this, the precipitation of ikaite from sea ice brines in the cooling phase of the system (autumn–winter) will conceivably depend on the rate of temperature change

(i.e., heat exchange in the ocean–ice–air system), which will cause, as a cascade of events, the physical concentration of solutes, the solubility changes of the polymorph, and also gas solubility changes in the sea ice brines. Added to this, the rate and extent of C_T loss from the brine via CO_2 degassing, which is related to the gas solubility changes, and via primary production will be of primary importance as independent mechanisms of compositional modification of the sea ice brines towards ikaite supersaturation and precipitation. Finally, the observed dissolution kinetics of ikaite suggest short turn-over time scales of the polymorph in corrosive solutions, such as surface oceanic water.

ACKNOWLEDGEMENTS

We are grateful to I11 beam line team, Prof. Tang and Drs. Lennie, Parker, and Thompson, and thank two anonymous reviewers for their helpful comments. The work was supported by NERC-UK (grant NE/F019289/1) and beam time awards EE-1471 and EE-1782 from Diamond Light Source Ltd.

REFERENCES

Arrigo K. R., Mock T. and Lizotte M. P. (2010) Primary producers and sea ice. In *Sea Ice* (eds. D. N. Thomas and G. S. Dieckmann), second ed. Wiley-Blackwell, Oxford, pp. 283–325.

Arrigo K. R., Worthen D. L., Lizotte M. P., Dixon P. and Dieckmann G. S. (1997) Primary production in Antarctic sea ice. *Science* **276**, 394–397.

Assur A. (1958) Composition of sea ice and its tensile strength in Arctic sea ice. *US Natl. Acad. Sci. Natl. Res. Council Publ.* **598**, 106–138.

Berner R. A., Westrich J. T., Graber R., Smith J. and Martens C. S. (1978) Inhibition of aragonite precipitation from supersaturated seawater: A laboratory and field study. *Am. J. Sci.* **278**, 816–837.

Bischoff J. L., Fitzpatrick J. A. and Rosenbauer R. J. (1993) The solubility and stabilization of ikaite ($CaCO_3{\cdot}6H_2O$) from 0 to 25 °C: Environmental and paleoclimatic implications for thinolite tufa. *J. Geol.* **101**, 21–33.

Burton E. A. and Walter L. M. (1987) Relative precipitation rates of aragonite and Mg calcite from seawater: temperature or carbonate ion control. *Geology* **15**, 111–114.

Busenberg E. and Plummer N. L. (1985) Kinetic and thermodynamic factors controlling the distribution of SO_4^{2-} and Na+ in calcites and selected aragonites. *Geochim. Cosmochim. Acta* **49**, 713–725.

Cox G. F. N. and Weeks W. F. (1983) Equations for determining the gas and brine volumes in sea ice samples. *J. Glaciol.* **29**, 306–316.

Davies K. J., Dove P. M. and De Yoreo J. J. (2000) The role of Mg^{2+} as an impurity in calcite growth. *Science* **290**, 1134–1137.

Delille B., Jourdain B., Borges A. V., Tison J.-L. and Delille D. (2007) Biogas (CO_2, O_2, dimethylsulfide) dynamics in spring Antarctic fast ice. *Limnol. Oceanogr.* **52**, 1367–1379.

Deming J. W. (2010) Sea ice bacteria and viruses. In *Sea Ice* (eds. D. N. Thomas and G. S. Dieckmann), second ed. Wiley-Blackwell, Oxford, pp. 247–282.

Dickson A. G. and Millero F. J. (1987) A comparison of the equilibrium constants for the dissociation of carbonic acid in seawater media. *Deep Sea Res.* **34**, 1733–1743.

Dieckmann G. S., Nehrke G., Papadimitriou S., Göttlicher J., Steininger R., Kennedy H., Wolf-Gladrow D. and Thomas D. N. (2008) Calcium carbonate as ikaite crystals in Antarctic sea ice. *Geophys. Res. Lett.* **35**, L08501. http://dx.doi.org/10.1029/2008GL033540.

Dieckmann G. S., Nehrke G., Uhlig C., Göttlicher J., Gerland S., Granskog M. A. and Thomas D. N. (2010) Brief communication: Ikaite ($CaCO_3{\cdot}6H_2O$) discovered in Arctic sea ice. *The Cryosphere* **4**, 227–230.

DOE (1994). In *Handbook of Methods for the Analysis of the Various Parameters of the Carbon Dioxide System in Sea Water; Version 2* (eds. C. Dickson and Goyet). ORNL/CDIAC-74.

Finneran D. W. and Morse J. W. (2009) Calcite dissolution kinetics in saline waters. *Chem. Geol.* **268**, 137–146.

Fischer M., Thomas D. N., Krell A., Nehrke G., Göttlicher J., Norman L., Meiners K. M., Riaux-Gobin C. and Dieckmann G. S. (2013) Quantification of ikaite in Antarctic sea ice. *Antarct. Sci.* **25**, 421–432.

Gehlen M., Bassinot F. C., Chou L. and McCorkle D. (2005) Reassessing the dissolution of marine carbonates. Part II: reaction kinetics. *Deep Sea Res. I* **52**, 1461–1476.

Geilfus N.-X., Delille B., Verbeke V. and Tison J.-L. (2012) Towards a method for high vertical resolution measurements of the partial pressure of CO_2 within bulk sea ice. *J Glaciol.* **58**, 287–300.

Gledhill D. K. and Morse J. W. (2006) Calcite dissolution kinetics in Na–Ca–Mg–Cl brines. *Geochim. Cosmochim. Acta* **70**, 5802–5813.

Gleitz M., Rutgers van der Loeff M., Thomas D. N., Dieckmann G. S. and Millero F. J. (1995) Comparison of summer and winter inorganic carbon, oxygen and nutrient concentrations in Antarctic sea ice brines. *Mar. Chem.* **51**, 81–91.

Hales B. and Emerson S. R. (1997) Evidence in support of first-order dissolution kinetics for calcite in seawater. *Earth Planet. Sci. Lett.* **48**, 317–327.

Hu Y.-B., Wolf-Gladrow D. A., Dieckmann G. S., Völker C. and Nehrke G. (2014) A laboratory study of ikaite ($CaCO_3{\cdot}6H_2O$) precipitation as a function of pH, salinity, temperature and phosphate concentration. *Mar. Chem.* **162**, 10–18.

Lee K., Kim T.-W., Byrne R. H., Millero F. J., Feely R. A. and Liu Y.-M. (2010) The universal ratio of boron to chlorinity for the North Pacific and North Atlantic oceans. *Geochim. Cosmochim. Acta* **74**, 1801–1811.

Leppäranta, M. and Manninen, T., 1988. The brine and gas content of sea ice with attention to low salinities and high temperatures. Finnish Institute Mar. Res. Int. Rep. 88-2.

Lopez O., Zuddas P. and Faivre D. (2009) The influence of temperature and seawater composition on calcite crystal growth mechanism and kinetics: implications for Mg incorporation in calcite lattice. *Geochim. Cosmochim. Acta* **73**, 337–347.

Marion G. M. (2001) Carbonate mineral solubility at low temperatures in the Na–K–Mg–Ca–H–Cl–SO_4–OH–HCO_3–CO_3–CO_2–H_2O system. *Geochim. Cosmochim. Acta* **65**, 1883–1896.

Mehrbach C., Culberson C. H., Hawley J. E. and Pytkowicz R. M. (1973) Measurement of the apparent dissociation constants of carbonic acid in seawater at atmospheric pressure. *Limnol. Oceanogr.* **18**, 897–907.

Miller L. A., Carnat G., Else B. G. T., Sutherland N. and Papakyriakou T. (2011a) Carbonate system evolution at the Arctic Ocean surface during autumn freeze-up. *J. Geophys. Res.* **116**, C00G04, doi: 10.1029/2011JC007143.

Miller L. A., Papakyriakou T. N., Collins R. E., Deming J. W., Ehn J. K., Macdonald R. W., Mucci A., Owens O., Raudsepp M. and Sutherland N. (2011b) Carbon dynamics in sea ice. A winter flux time series. *J. Geophys. Res.* **116**, C02028. http://dx.doi.org/10.1029/2009JC006058.

Millero F. J. (1995) Thermodynamics of the carbon dioxide system in the oceans. *Geochim. Cosmochim. Acta* **59**, 661–677.

Millero F. J. and Huang F. (2009) The density of seawater as a function of salinity (5 to 70 g kg^{-1}) and temperature (273.15 to 363.15 K). *Ocean Sci.* **5**, 91–100.

Morse J. W., Arvidson R. S. and Lüttge A. (2007) Calcium carbonate formation and dissolution. *Chem. Rev.* **107**, 342–381.

Mucci A. (1983) The solubility of calcite and aragonite in seawater at various salinities, temperatures, and one atmosphere total pressure. *Am. J. Sci.* **283**, 780–799.

Munro D. R., Dunbar R. B., Mucciarone D. A., Arrigo K. R. and Long M. C. (2010) Stable isotopic composition of dissolved inorganic carbon and particulate organic carbon in sea ice from the Ross Sea, Antarctica. *J. Geophys. Res.* **115**, C09005. http://dx.doi.org/10.1029/2009JC005661.

Papadimitriou S., Kennedy H., Kennedy P. and Thomas D. N. (2013) Ikaite solubility in seawater-derived brines at 1 atm and sub-zero temperatures to 265 K. *Geochim. Cosmochim. Acta* **109**, 241–253.

Papadimitriou S., Kennedy H., Norman L., Kennedy D. P. and Thomas D. N. (2012) The effect of biological activity, $CaCO_3$ mineral dynamics, and CO_2 degassing in the inorganic carbon cycle in sea ice in late winter-early spring in the Weddell Sea, Antarctica. *J. Geophys. Res.* **117**, C08011. http://dx.doi.org/10.1029/2012JC008058.

Papadimitriou S., Kennedy H., Kattner G., Dieckmann G. S. and Thomas D. N. (2004) Experimental evidence for carbonate precipitation and CO_2 degassing during sea ice formation. *Geochim. Cosmochim. Acta* **68**, 1749–1761.

Papadimitriou S., Thomas D. N., Kennedy H., Haas C., Kuosa H., Krell H. and Dieckmann D. S. (2007) Biogeochemical composition of natural sea ice brines from the Weddell Sea during early austral summer. *Limnol. Oceanogr.* **52**, 1809–1823.

Petrich C. and Eicken H. (2010) Growth, structure, and properties of sea ice. In *Sea Ice* (eds. D. N. Thomas and G. S. Dieckmann), second ed. Wiley-Blackwell, Oxford, pp. 23–77.

Pierrot D., Neill C., Sullivan K., Castle R., Wanninkhof R., Lüger H., Johannessen T., Olsen A., Feely R. A. and Cosca C. E. (2009) Recommendations for autonomous underway pCO_2 measuring systems and data-reduction routines. *Deep Sea Res. II* **56**, 512–522.

Ricker W. E. (1973) Linear regressions in fishery research. *J. Fish. Res. Board Can.* **30**, 409–434.

Rysgaard S., Glud R. N., Lennert K., Cooper M., Halden N., Leakey R. J. G., Hawthorne F. C. and Barber D. (2012) Ikaite crystals in melting sea ice – implications for pH and pCO_2 levels in Arctic surface waters. *The Cryosphere* **6**, 901–908.

Rysgaard S., Sogaard D. H., Cooper M., Pucko M., Lennert K., Papakyriakou T. N., Wang F., Geilfus N. X., Glud R. N., Ehn J., McGinnis D. F., Attard K., Sievers J., Deming J. W. and Barber D. (2013) Ikaite crystal distribution in winter sea ice and implications for CO_2 system dynamics. *The Cryosphere* **7**, 707–718.

Weiss R. S. (1974) Carbon dioxide in water and seawater: The solubility of a non-ideal gas. *Mar. Chem.* **2**, 203–215.

Zhong S. and Mucci A. (1993) Calcite precipitation in seawater using the constant addition technique: a new overall reaction kinetic expression. *Geochim. Cosmochim. Acta* **57**, 1409–1417.

Zuddas P. and Mucci A. (1998) Kinetics of calcite precipitation from seawater. II. The influence of ionic strength. *Geochim. Cosmochim. Acta* **62**, 757–766.

Zuddas P., Pachana K. and Faivre D. (2003) The influence of dissolved humic acids on the kinetics of calcite precipitation from seawater solutions. *Chem. Geol.* **201**, 91–101.

Associate editor: Robert H. Byrne